JGR Biogeosciences

RESEARCH ARTICLE
10.1029/2019JG005534

Key Points:
- Reflected near-infrared radiation is a strong proxy for canopy photosynthesis
- This proxy works for a wide range of ecosystem structure and function
- The method has promise to be used for a variety of applications relating to carbon and water use

Supporting Information:
- Supporting Information S1

Correspondence to:
D. D. Baldocchi,
baldocchi@berkeley.edu

Citation:
Baldocchi, D. D., Ryu, Y., Dechant, B., Eichelmann, E., Hemes, K., Ma, S., et al. (2020). Outgoing near-infrared radiation from vegetation scales with canopy photosynthesis across a spectrum of function, structure, physiological capacity, and weather. *Journal of Geophysical Research: Biogeosciences*, *125*, e2019JG005534. https://doi.org/10.1029/2019JG005534

Received 23 OCT 2019
Accepted 23 APR 2020
Accepted article online 25 APR 2020

Author Contributions:
Conceptualization: Dennis D. Baldocchi, Youngryel Ryu, Benjamin Dechant, Grayson Badgley, Yelu Zeng, Joseph A. Berry
Data curation: Camilo Rey Sanchez, Robert Shortt, Daphne Szutu, Joe Verfaillie
Formal analysis: Dennis D. Baldocchi
Funding acquisition: Dennis D. Baldocchi
Investigation: Dennis D. Baldocchi
Methodology: Dennis D. Baldocchi, Youngryel Ryu, Benjamin Dechant, Joe Verfaillie, Grayson Badgley, Yelu Zeng, Joseph A. Berry
Project administration: Dennis D. Baldocchi
Resources: Dennis D. Baldocchi
Software: Dennis D. Baldocchi
Supervision: Dennis D. Baldocchi
Validation: Dennis D. Baldocchi, Elke Eichelmann, Kyle Hemes, Siyan Ma, Camilo Rey Sanchez, Robert Shortt,
(continued)

Outgoing Near-Infrared Radiation From Vegetation Scales With Canopy Photosynthesis Across a Spectrum of Function, Structure, Physiological Capacity, and Weather

Dennis D. Baldocchi[1], Youngryel Ryu[2], Benjamin Dechant[2], Elke Eichelmann[1], Kyle Hemes[1], Siyan Ma[1], Camilo Rey Sanchez[1], Robert Shortt[1], Daphne Szutu[1], Alex Valach[1], Joe Verfaillie[1], Grayson Badgley[3], Yelu Zeng[3], and Joseph A. Berry[3]

[1]Department of Environmental Science, Policy and Management, University of California, Berkeley, CA, USA, [2]Department of Landscape Architecture and Rural Systems Engineering, Seoul National University, Seoul, South Korea, [3]Department of Global Ecology, Carnegie Institution for Science, Stanford, CA, USA

Abstract We test the relationship between canopy photosynthesis and reflected near-infrared radiation from vegetation across a range of functional (photosynthetic pathway and capacity) and structural conditions (leaf area index, fraction of green and dead leaves, canopy height, reproductive stage, and leaf angle inclination), weather conditions, and years using a network of field sites from across central California. We based our analysis on direct measurements of canopy photosynthesis, with eddy covariance, and measurements of reflected near-infrared and red radiation from vegetation, with light-emitting diode sensors. And we interpreted the observed relationships between photosynthesis and reflected near-infrared radiation using simulations based on the multilayer, biophysical model, CanVeg. Measurements of reflected near-infrared radiation were highly correlated with measurements of canopy photosynthesis on half-hourly, daily, seasonal, annual, and decadal time scales across the wide range of function and structure and weather conditions. Slopes of the regression between canopy photosynthesis and reflected near-infrared radiation were greatest for the fertilized and irrigated C_4 corn crop, intermediate for the C_3 tules on nutrient-rich organic soil and nitrogen fixing alfalfa, and least for the native annual grasslands and oak savanna on nutrient-poor, mineral soils. Reflected near-infrared radiation from vegetation has several advantages over other remotely sensed vegetation indices that are used to infer canopy photosynthesis; it does not saturate at high leaf area indices, it is insensitive to the presence of dead legacy vegetation, the sensors are inexpensive, and the reflectance signal is strong. Hence, information on reflected near-infrared radiation from vegetation may have utility in monitoring carbon assimilation in carbon sequestration projects or on microsatellites orbiting Earth for precision agriculture applications.

1. Introduction

Canopy photosynthesis by ecosystems is the foremost input of carbon into carbon cycle models that are linked to state-of-the-art climate simulations (Bonan & Doney, 2018; Prentice et al., 2000). Unfortunately, the state of simulating photosynthesis at ecosystem to global scales remains poor (Ryu et al., 2019; Schaefer et al., 2012). This raises a philosophical question: "If we are unable to simulate ecosystem photosynthesis accurately, across a spectrum of time and space scales, how can we have faith in how that carbon is being allocated as it travels through the carbon cycle?"

To improve model simulations of canopy photosynthesis, we need unbiased and representative empirical estimates that are compatible with models across a spectrum of time and space. How does one infer canopy photosynthesis of ecosystems better and use this information to upscale to continental and global scales? There is a hierarchy of bottom-up and top-down approaches that have particular strengths and weakness across a range of temporal and spatial scales (Canadell et al., 2000). Eddy covariance method measures canopy photosynthesis directly, but it needs handshaking with remote sensing to upscale assimilatory carbon fluxes to scales larger than flux footprints (Falge et al., 2002; Running et al., 1999). The simplest, and most widely used, method to infer photosynthesis is the light use efficiency model. It quantifies canopy photosynthesis as the product of photon flux density of incoming visible sunlight (Q_P) times the fraction

Daphne Szutu, Alex Valach, Joe Verfaillie

Visualization: Dennis D. Baldocchi
Writing - original draft: Dennis D. Baldocchi
Writing – review & editing: Youngryel Ryu, Benjamin Dechant, Elke Eichelmann, Kyle Hemes, Siyan Ma, Alex Valach, Grayson Badgley, Yelu Zeng, Joseph A. Berry

of that light absorbed by green vegetation ($f_{a,P}$) times a light use efficiency (ϕ) (Prince & Goward, 1995; Ruimy et al., 1996; Zhao et al., 2005). This approach has been used to upscale canopy photosynthesis to landscape, regional, and global space scales and on to daily to decadal time scales using reflected sunlight measured by sensors on satellites (Field et al., 1995; Running et al., 2004). However, to do so, we must know how $f_{a,P}$ varies with leaf area index and how light use efficiency varies with environmental stresses. The reality remains that light use efficiency models require calibration, optimization, and tuning of two parameters at representative sites with direct flux measurements and site metadata in order to compute canopy photosynthesis with high enough fidelity (Heinsch et al., 2006; Running et al., 1999; Yuan et al., 2007).

How else can we estimate or infer canopy photosynthesis? A classic theoretical study (Sellers, 1987; Sellers et al., 1992) found that the flux density of absorbed visible light is proportional to the flux density of near-infrared radiation reflected by the vegetation. In recent years, a set of papers found that daily integrated canopy photosynthesis is proportional to the reflectance of near-infrared radiation of green leaves of a canopy, as detected by sensors on satellites (Badgley et al., 2017; Badgley et al., 2019). Another set of papers has interpreted these results by examining how reflected near-infrared radiation is related to absorbed visible light (Dechant et al., 2020; Zeng et al., 2019). These findings have the potential for establishing a paradigm shift in how we estimate canopy photosynthesis, without tuning. But tests at the field scale between direct measurements of canopy photosynthesis and reflected near-infrared radiation from vegetation are needed.

In field conditions, canopy photosynthesis varies on a diel basis due to changes in solar radiation, temperature, and humidity deficits. And canopy photosynthesis varies seasonally due to changes in climate, phenology, and soil moisture. This prompts us to ask how well canopy photosynthesis is related to near-infrared reflectance across a spectrum of time scales and variations in ecosystem structure, function, and physiological capacity. In this paper, we evaluate the relation between direct measurements of canopy photosynthesis and reflected near-infrared radiation from a contrasting set of agricultural and native ecosystems. This evaluation is based on data from a network of eddy covariance sites in California which experience similar weather and climate but possess a range of canopy structural and functional properties and physiological capacity. First, we explore data from an annual corn (*Zea mays*) crop; it uses the C_4 photosynthetic pathway, it is irrigated, it is growing on nutrient-rich organic soils, it is fertilized, it experiences a wide range of leaf area index and canopy coverage over its life cycle, and its tall canopy and erect leaves trap photons effectively. Second, we explore data from a tule/cattail (*Typha* spp. and *Schoenoplectus acutus*) wetland. This ecosystem, and the remaining cases, uses the C_3 photosynthetic pathway. In addition, the tule/cattail wetland is perennial and deciduous, it contains a mixture of green and dead vegetation, it has erect stems, and it is flooded. Third, we explore data from an alfalfa (*Medicago sativa*) field. This perennial, nitrogen-fixing agroecosystem is irrigated, and it undergoes multiple cuttings over the year, which changes its leaf area index and fraction of absorbed sunlight. Finally, we explore data from two native ecosystems, an annual (*Bromus* spp., *Avena* spp., *Hordeum* spp., and *Festuca* spp.) grassland and an oak (*Quercus douglasii*) savanna. The annual grassland is a grazed, native ecosystem that experiences a wet, cool growing season, during the late winter and spring. Afterward, it experiences seasonal drought in the late spring after the rains stop. And the vegetation is dead during much of the rainless summer and early autumn. This ecosystem experiences a wide range in leaf area index and photosynthetic capacity as the soil moisture reservoir fills and becomes depleted (Ma et al., 2016). The oak savanna is the most complex and heterogeneous canopy. It is composed of an overstory of scattered, deciduous oak trees and an understory of grass. The oak trees are physiologically active between April and September during the hot, summer, after the rains have ceased (Ma et al., 2016). The trees experience physiological stress over the summer as the soil moisture reservoir becomes depleted, and the understory grass is dead.

Another reason we are conducting this research is to provide an alternative proxy for canopy photosynthesis that is inexpensive and whose application does not suffer from technical challenges that are associated with measuring solar-induced fluorescence and carbon fluxes with eddy covariance. If proven effective, this inferred approach has potential to be used to evaluate photosynthesis of carbon sequestration projects, which may serve as natural carbon solutions (Griscom et al., 2017). Or cheap radiation sensors can be mounted on microsatellites (CubeSats) orbiting the Earth and used for agricultural and ecological management (Aragon et al., 2018).

2. Materials and Methods

2.1. Field Sites

The locations and vegetation of the sites are listed in Table 1. These are Ameriflux sites with publicly available data. Many of the details of the sites, their vegetation, and soil properties are reported in prior papers by this group (Eichelmann et al., 2018; Hemes et al., 2019; Ma et al., 2016) or are accessible through the respective Ameriflux web sites. The agricultural and wetland sites in the Sacramento-San Joaquin Delta are on highly organic soils with high nitrogen content (1% to 2%). The savanna and grassland sites are on mineral soils with much lower nitrogen (0.1%).

2.2. Eddy Covariance and Meteorological Measurements

We used the eddy covariance method to measure flux densities of sensible and latent heat and carbon dioxide between vegetation and the atmosphere (Baldocchi, 2003). The set of sites are ideal from the perspective of applying micrometeorological theory and the eddy covariance method; they are flat, they experience vigorous winds from a preferred direction, and they possess extended fetches.

Implementing the eddy covariance method requires that we measure the covariance between fluctuations in vertical velocity and trace gas mixing ratio. The sensor system measures three-dimensional wind velocities (horizontal, u; lateral, v; vertical, w; m s^{-1}) and temperature (T_{sonic}) with a sonic anemometer (Gill Wind Master Pro; Gill Instruments Ltd, Lymington, Hampshire, England). Fluctuations in CO_2 and H_2O molar density (ρ_{CO_2} and ρ_{H_2O}) were measured with an open-path infrared gas analyzer (LI-7550A; LI-COR Biogeosciences, Lincoln NE, USA).

The eddy covariance instrument systems and meteorological and light sensors were mounted on scaffold towers. Depending upon the height of the vegetation, the sensors were mounted between 3 and 5 m above the ground at the agricultural and grassland sites. The instruments were mounted at 20 m over the savanna. Depending upon the time of day, the preferred upwind fetch ranged between 450 and 2,000 m (Eichelmann et al., 2018; Kim et al., 2006).

Sampling theory requires that we measure the contributions of the fastest to slowest eddies. Covariances between scalars (CO_2; temperature, T; and humidity, q) and vertical velocity (w) were computed by sampling fluctuations 20 times per second and averaging for 30 min. We applied a series of standard corrections using in-house software (Eichelmann et al., 2016; Hemes et al., 2019) Coordinate rotations were applied to align the streamlines with the surface at the site resulting in zero mean w and v within each 30-min average. When using open-path sensors, the effects of fluctuations in air density by temperature and moisture need to be considered (Webb et al., 1980). Sonic temperature, T_{sonic}, fluctuations were calculated from fluctuations in the speed of sound after crosswind and humidity corrections are applied. No high-frequency spectral corrections were applied to fluxes computed using open-path sensors since cospectral analysis indicated that flux losses were less than 5% (Detto et al., 2011; Knox et al., 2015), which is within the accuracy of any spectral correction algorithm; we designed the system sampling rates and sensor placement (height and separation) to minimize such corrections.

Fluxes were filtered for spikes in half-hour average densities, variances, covariances, and nonstationary conditions. We filled the missing data with neural network and gap-filling methods using meteorological variables as inputs (Moffat et al., 2007).

A suite of meteorological variables was measured in conjunction with the mass and energy flux measurements. Air temperature and relative humidity were measured with an aspirated and shielded thermistor and capacitance sensor (Vaisala, models HMP 45 and HMP 60, Woburn, MA). We measured incoming and outgoing shortwave and longwave radiation with Hukseflux (model NR01) and Kipp and Zonen (model CNR1) net radiometers. Soil and water temperatures were measured with a profile of copper-constantan thermocouples. Soil moisture was measured with a network of capacitance (Theta Probe ML3, Delta-T Devices, Cambridge, UK) sensors.

Total photosynthetically active radiation (PAR_{total}) measurements were made with upward facing, boom-affixed, quantum sensors (Kipp & Zonen, PAR-Lite or PQS1) at each tower. Diffuse PAR ($PAR_{diffuse}$) was measured with a homebuilt rotating shadow band. The quantum sensor was periodically shaded (approximately once per minute) by a shadow band that rotated around the sensor (Michalsky et al., 1986). This

Table 1
List of Ameriflux Eddy Covariance Sites Operated by the Berkeley Biometeorology Lab

Site ID	Vegetation	Latitude, N	Longitude, W	AmeriFlux site
US-Bi1	alfalfa	38.102	121.504	https://ameriflux.lbl.gov/sites/siteinfo/US-Bi1
US-Bi2	corn	38.109	121.535	https://ameriflux.lbl.gov/sites/siteinfo/US-Bi2
US-Tw1	wetland	38.107	121.647	https://ameriflux.lbl.gov/sites/siteinfo/US-Tw1
US-Ton	Oak savanna	38.431	120.965	https://ameriflux.lbl.gov/sites/siteinfo/US-Ton
US-Var	Annual grassland	38.41	120.95	https://ameriflux.lbl.gov/sites/siteinfo/US-Var

sensor was sampled at 2 Hz resulting in several measurements each time the shadow passed over the sensor. The minimum PAR measured during one full cycle of the shadow band was recorded and stored in 30-min averages as $PAR_{diffuse.}$

We evaluated canopy height using the aerodynamic method (Chu et al., 2018; Pennypacker & Baldocchi, 2015). A digital camera monitored the phenological status of the vegetation and field management, through the computation of the greenness index or gap fraction (Ryu et al., 2012; Sonnentag et al., 2012). Time series of canopy height of the agricultural crops are presented in supporting information Figures S1 and S2.

Reflected near-infrared radiation was measured with Decagon SRS-Ni NDVI sensors mounted on towers near the flux equipment. An advantage of tower-based reflectance sensors is that no atmospheric corrections were needed. These sensors measure incident or reflected radiation in two bands in energy units. The sensor bands were centered at 630 and 800 nm with 50 and 40 nm full width half maximum, respectively. Normalized Difference Vegetation Index, NDVI, was computed as the difference between the near-infrared (NIR, 800 nm) and red (630 nm) reflectance divided by the sum of the NIR and red reflectance (Tucker, 1979). To increase the area of the footprint viewed by the sensors and minimize biases between sites, we used the hemispherical view setting. The sensors were mounted on extended booms from the main tower and were several meters above the vegetation. We deployed these sensors at various sites in 2017, 2018, and 2019.

Reflected near-infrared radiation from the vegetation, NIR_v, was calculated in terms of a renormalized NDVI times reflected NIR; NDVI was renormalized by setting its minimum value to 0 and its maximum value to 1, effectively, subtracting off the soil component (Zeng et al., 2019).

To examine decadal relationships between near-infrared radiation and ecosystem photosynthesis, we extracted data from a homemade sensor that measured the reflectance of red and near-infrared radiation with light-emitting diodes (Ryu et al., 2010). We assumed that the flux density of reflected near-infrared radiation was one-half incoming shortwave radiation (Ross, 1980) times the reflectance of near-infrared radiation. The homemade sensor was calibrated with periodic comparisons with an Ocean Optics spectrometer (Ryu et al., 2010).

2.3. CanVeg Model Simulations

We applied the biophysical CanVeg model to interpret the mechanisms by which canopy photosynthesis may or may not respond to NIR_v. The CanVeg model is a canopy photosynthesis and evaporation model that has been described and validated elsewhere (Baldocchi et al., 1999; Baldocchi & Meyers, 1998; Oikawa et al., 2017). CanVeg computes the microclimate of a canopy by considering the radiative transfer of visible, near-infrared, and longwave photons through a multilayer, one-dimensional canopy (Norman, 1979). For the computations of radiative transfer through the vegetation, we applied Beer's law and assumed a spherical leaf inclination angle distribution; the mean direction cosine between the mean leaf normal and the Sun (G) has a value of 0.5 (Ross, 1980). Turbulent transport of gases between leaves and the atmosphere was considered using a Lagrangian turbulent transfer theory (Raupach, 1989). Based on the computation of micrometeorological conditions, the CanVeg model computes leaf energy balance (Paw, 1988), photosynthesis (Farquhar et al., 1980) and stomatal conductance (Collatz et al., 1991) on the sunlit and shaded fractions of each layer in the canopy (Norman, 1981). Information on the fluxes and turbulent mixing was used to

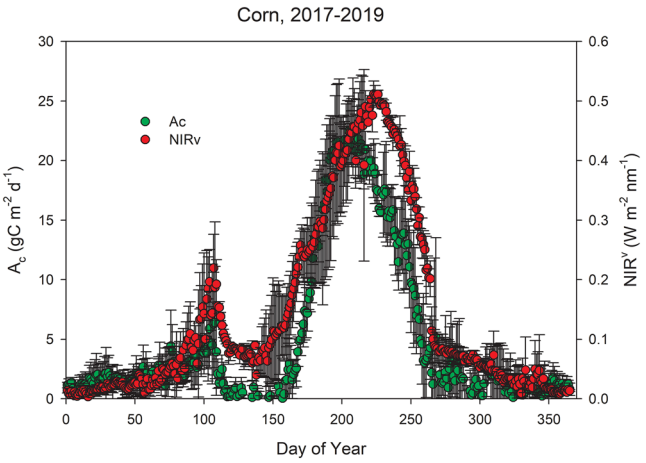

Figure 1. Daily variation in daily integrated canopy photosynthesis (A_c) and the flux density of near-infrared radiation reflected by vegetation, NIR_v during midday. The data were measured over a corn canopy during the years 2017 through 2019. NIRv data were averaged for the midday (1000 to 1400) period of each day.

compute scalar fields (temperature, humidity, and carbon dioxide). Flux profiles were recomputed with new information on concentration fields. Iteration between flux and concentration fields continue until steady state. Simulations were made, using CanVeg, for an ideal alfalfa canopy and weather inputs from the 2018 growing season.

3. Results

In the following, we explore the relationship between measurements of canopy photosynthesis and reflected near-infrared radiation from vegetation for a suite of cases, varying in function and structure.

3.1. C_4 Photosynthesis, Corn

A corn canopy is a good test for the utility of using NIR_v as a proxy for canopy photosynthesis because it achieves high rates of photosynthesis and it experiences a wide range in height and leaf area index over the growing season. These attributes influence how well photons are trapped and reflected by vegetation (Ross, 1980) and how the captured photons modulate canopy photosynthesis.

Figure 1 shows the seasonal pattern of daily integrated canopy photosynthesis, A_c, and mean midday (1000 through 1400 hours) flux density of near-infrared radiation reflected from the green vegetation; these data were averaged each day over the 3-year period, 2017–2019. During this time period, the structure of the corn canopy varied from (1) seedling stage, with wide open rows; (2) a closed canopy, 3 m tall, with a leaf area index reaching 4.2; (3) a reproductive stage, with tassels and ears; and (4) senescence.

In general, we observed strong temporal correlation (Table 2) between A_c and NIR_v ($r^2 = 0.84$). During the 2017 through 2019 growing seasons, daily integrated corn photosynthesis ranged between 0 and 30 gC m^{-2} day^{-1}, and reflected near-infrared radiation from vegetation ranged between 0 and 0.6 W m^{-2} nm^{-1}. Close inspection of Figure 1 reveals that there was a phase difference between A_c and NIR_v, with A_c leading during the middle to late growing season. Inspection of phenocam images reveals that the downturn in A_c occurred when the corn began to tassel, around Day 210 (supporting information Figure S3). Subsequently, the downturn in NIR_v occurred around Day 234. This occurred when the canopy tasseling was complete, which is when this reproductive organ competed most with leaves for capturing photons. It is also noteworthy that the NIR_v sensors detected springtime bumps (approximately Day 100) in canopy photosynthesis. This was due to weeds growing after the winter flood waters receded and before the soil was cultivated and planted in corn.

How well does reflected near-infrared radiation from vegetation match canopy photosynthesis on shorter time scales? A one-to-one plot between half-hour averages of canopy photosynthesis, A_c, and NIR_v is shown in Figure 2. We observe a linear relationship (slope was 98.3 (μmol m^{-2} s^{-1})/(W m^{-2} nm^{-1})) and high correlation ($r^2 = 0.818$) between these two variables at short time intervals. It is noteworthy that simple measurements of the flux density of reflected NIR_v were able to resolve changes in canopy photosynthesis that were simultaneously being modulated by variations in sunlight, temperature, and vapor pressure deficit and changes in leaf area index, reproduction state, senescence, and fraction of soil exposure. We also note that linearity holds well across a wide range of photosynthesis and does not become saturated like it does with other vegetation indices, such as reflected NIR from the soil and vegetation and NDVI (Sellers, 1985); see supporting information Figures S4 and S5.

3.2. C_3 Photosynthesis With a Mixture of Green and Dead Vegetation, Tule/Cattail Wetland

The tule/cattail wetland is a good case to compare with corn, as it too is apt to trap photons effectively; it is tall (~3 m), it possesses a high plant area index (greater than 6), and it possesses erect leaf orientation. And because the wetland is flooded, it provides us with a case with little reflectance from the "soil" as the water is dark. On the other hand, the wetland also retains much legacy dead vegetation (Dronova & Taddeo, 2016;

Table 2
Regression Statistics Between Canopy Photosynthesis and Reflected Near-Infrared Radiation From Vegetation

Field site	Half-hour time step slope (μmol m^{-2} s^{-1})/(W m^{-2} nm^{-1})	R^2	
Corn	98.3	0.818	
Tule/cattails	74.1	0.869	
alfalfa	81.0	0.841	
Oak savanna	54.2	0.447	
Annual grassland	59.0	0.803	
	Daily time step		
	gC m^{-2} day^{-1}/W m^{-2} nm^{-1}		A_{max} gC m^{-2} day^{-1}
Corn, 2017	45.5	0.742	24.9
Corn, 2018	39.7	0.848	24.6
Corn, 2019	32.7	0.757	21.1
Tule/Cattails, 2018	33.0	0.943	14.4
Tule/Cattails, 2019	45.2	0.886	10.4
Alfalfa, 2018	29.5	0.818	18.1
Alfalfa, 2019	38.0	0.859	21.0
Oak savanna, 2018–2019	28.2	0.711	9
Annual grassland, 2019	27.4	0.880	10.2
	μmol m^{-2} s^{-1}/W m^{-2}		
CanVeg, LAI = 1	0.133	0.852	21.2
CanVeg, LAI = 2	0.128	0.924	28.5
CanVeg, LAI = 3	0.119	0.945	31.3
CanVeg, LAI = 4	0.117	0.962	33.3
CanVeg, LAI = 4, 0.8 *V_{cmax}	0.105	0.931	33.1
CanVeg, LAI = 4, 0.6 *V_{cmax}	0.0925	0.877	32.3

Note. Statistics include slopes from half-hour averages between A_c and NIR$_v$ and of daily integrals of canopy photosynthesis versus midday (1000 to 1400 hours) mean values of NIRv. Slope is the regression slope between Ac and NIRv. R^2 is the coefficient of determination; A_{max} is the maximum daily flux of canopy photosynthesis. Listed are regression slopes and the coeficient of determination (r^2). For daily time steps we also list maximum photosynthesis over the growing season (A_{max}). Data are presented for measurements in the field and for computations based on the CanVeg model.

Rocha et al., 2008; Taddeo & Dronova, 2018), which can complicate the estimated canopy photosynthesis with light use efficiency models, which is based on the green leaves that intercept sunlight.

Figure 3 shows the seasonal pattern of daily integrated canopy photosynthesis, A_c, and mean near-infrared radiation reflected from the green vegetation for two contrasting years. Both measures experienced a high correlation between one another ($r^2 = 0.94$ in 2018 and $r^2 = 0.88$ in 2019). Carbon assimilation fluxes and reflected NIR$_v$ followed a similar seasonal pattern of increasing in the spring, then decreasing photosynthesis into the autumn, and near-zero values during the winter dormant period. During 2018, wetland photosynthesis ranged between 0 and 15 gC m^{-2} day^{-1} and reflected near-infrared radiation from vegetation ranged between 0 and 0.35 W m^{-2} nm^{-1}. However, we observed a slight phase shift between the two time series during the 2018 growing season, with canopy photosynthesis decreasing more quickly than NIR$_v$; this period corresponded to the period of smoke and higher diffuse fraction (Hemes et al., 2020) which affects how photons are trapped by the vegetation (Knohl & Baldocchi, 2008). During 2019, the water table of the wetland was not maintained. Consequently, we observed much lower sums of daily integrated photosynthesis and reflected near-infrared radiation from green vegetation.

The one-to-one plot between half-hour measurements of A_c and NIR$_v$ revealed a linear relationship with a very high correlation among one another ($r^2 = 0.87$) across the contrasting years; the slope between the two variables was 74.1 (μmol m^{-2} s^{-1})/(W m^{-2} nm^{-1}) (Figure 4). Again, these data support the hypothesis that

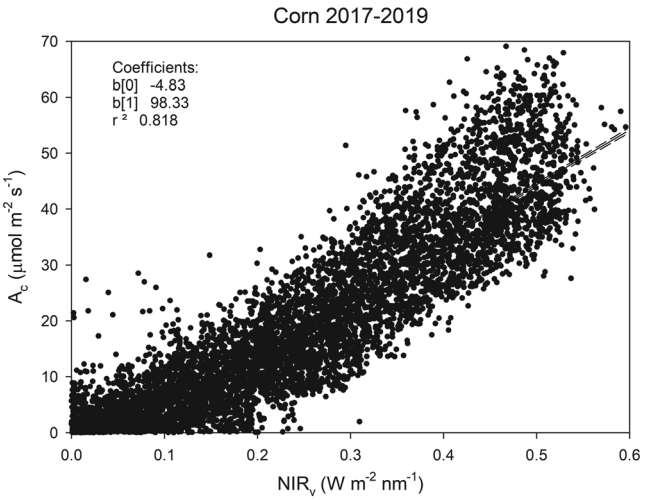

Figure 2. Plot between 30-min averages of canopy photosynthesis, A_c, and NIR_v. NIR_v is the flux density of near-infrared radiation reflected by the vegetation. These data are from Days 150 through 270 during 2017 through 2019. The coefficient of variation (r^2) is 0.818. The slope between these two variables is 98.3 (μmol m^{-2} s^{-1})/(W m^{-2} nm^{-1}).

NIR_v is able to predict canopy photosynthesis as temperature, humidity, water table, and the fraction of green to dead vegetation vary over the course of the growing season.

3.3. C_3 Photosynthesis of Alfalfa, With Varying Leaf Area Index

Alfalfa is an ideal test case for examining the relationship between A_c and NIR_v because the canopy experiences multiple cuttings over the course of the year, which abruptly modulates its leaf area index; between cuttings leaf area index ranged between 0 and 3. At this study site, we experienced six sets of cuttings during 2018, which forced A_c to range between 0 and 20 gC m^{-2} day^{-1} and average NIR_v to range between 0 and 0.35 W m^{-2} nm^{-1} (Figure 5). In general, we observed tight coherence and correlation (r^2 = 0.82) between the ups and downs in both A_c and NIR_v through each cutting cycle. Data from 2019 are not shown here, but they show similar behavior.

Figure 6 shows the comparison between A_c and NIR_v for half-hour measurements over the repeated cycling of growth, cutting, and regrowth over two years, 2018–2019. Like for the case of corn and tule/cattail wetlands, we observe a strong correlation and a linear response between the independent and dependent variables for the wide range of structural conditions experienced by the alfalfa canopy over the year (r^2 = 0.841, slope = 81.1). In contrast, NDVI does not capture the variations in A_c well (supporting information Figure S6).

3.4. C_3 Photosynthesis of Native Vegetation That Experiences Seasonal Drought

3.4.1. Annual Grassland

Over the course of the year, the annual grassland experiences a cool winter growing season, with rapid growth after the last frost in March and then senescence and death after the last rains occur in April (Ma et al., 2016). By June, the grass is dead and photosynthesis ceases, until rains resume in the autumn. Figure 7 shows that NIR_v tracks the seasonal change in canopy photosynthesis through this wide range of phenoseasons with high fidelity, yielding a strong correlation between the two variables (r^2 = 0.88).

Figure 8 shows the one-to-one plot between A_c and NIR_v at the 30 min time scale. Despite a wide range in meteorological and soil moisture conditions, the correlation between A_c and NIR_v remained relatively high (r^2 = 0.804); this performance was on par with what we observed over the agricultural crops and wetlands (r^2 > 0.8). On the other hand, the slope of this relationship was noticeably lower than those for the managed crops and wetland, which experience higher photosynthetic capacity due to fertilization, irrigation, nitrogen fixation, and/or higher N in their organic soils.

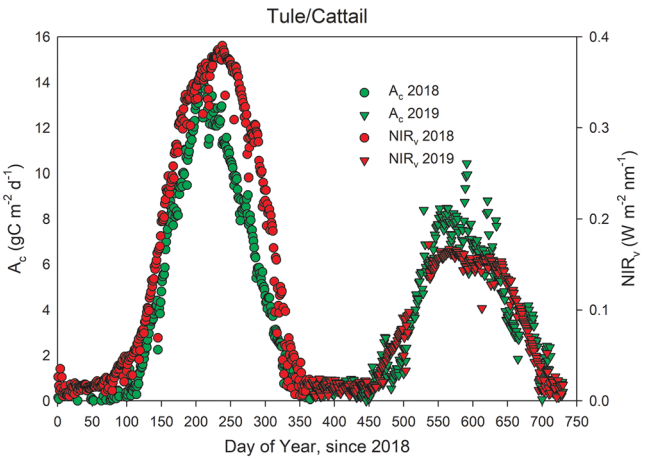

Figure 3. Seasonal patterns of daily integrated canopy photosynthesis (A_c) and reflected NIR from vegetation (NIR_v) plotted by day of year over tule/cattail wetland for years 2018 and 2019.

3.4.2. Oak Savanna

The oak savanna provides an interesting test of the links between A_c and NIR_v because the canopy is spatially heterogeneous (Béland et al., 2014; Chen et al., 2007) and it experiences seasonal water deficits (Baldocchi et al., 2004). Over the growing season air temperature ranged between 0 and 40°C, volumetric soil moisture ranged between 0.10 and 0.4 m^3 m^{-3}, and photosynthetic capacity ranged between 25 and 125 μmol m^{-2} s^{-1} (Osuna et al., 2015; Xu & Baldocchi, 2003). Figure 9 shows very high fidelity between the time series of daily integrated canopy photosynthesis and mean NIR_v for 2018 and 2019; the coefficient of determination (r^2) between these two variables is 0.71. Both variables experience a ramp up in values in the spring, when photosynthetic capacity is highest and soil moisture and temperature conditions are moderate. Then both variables experience a rapid decline during

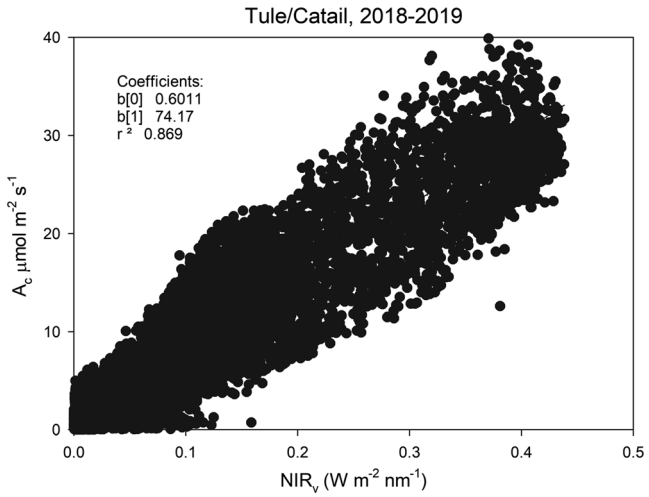

Figure 4. Plot between 30-min averages of canopy photosynthesis, A_c, and NIR_v during 2018 and 2019. The coefficient of variation (r^2) is 0.869. The slope between these two variables is 74.2 (µmol m^{-2} s^{-1})/(W m^{-2} nm^{-1}).

the hot, rainless summer as soil moisture reservoir is depleted. It is worth noting that NIR_v corresponded well with A_c through the growing season despite the wide range in photosynthetic capacity that the trees experience (Osuna et al., 2015; Xu & Baldocchi, 2003).

The comparison between half-hour average canopy photosynthesis and NIR_v reflectance values, on the other hand, experience much scatter, compared to the other sites (Figure 10; slope = 54.2; r^2 = 0.447). We suspect differences in the footprints sampled by the light sensors and that of the eddy covariance measurements, over this spatially heterogeneous canopy, may degrade the correlation between these two variables on short time scales; the savanna is composed of widely spaced trees and underlying grass that is either green or dead.

4. Discussion

In this analysis, we found that well-watered crops, wetland vegetation, annual grasslands, and savanna experienced a strong linear relation between A_c and NIR_v. Except for the heterogeneous savanna, all experienced relationships having a coefficient of variation, r^2, greater than 0.80 when examined on half-hourly and daily time scales (Table 2). This linear and well-correlated behavior was robust across a range of function (C_3 and C_4 photosynthesis), structure (fraction of green and dead leaves, variable leaf area index and leaf angles, and reproductive state), and physiological capacity (nitrogen fixing, fertilized, high and low soil N, and high and low soil moisture).

We conclude that this strong linearity across many conditions is a marked improvement over the performance of light use efficiency models; in comparison, light use efficiency models require tuning of the fraction of absorbed light for variations in fraction of green and dead leaves and tuning of light use efficiency for variations in physiological stresses to achieve this level of performance (Heinsch et al., 2006; Yuan et al., 2007).

Use of hemispherical view on the outgoing near-infrared radiation sensors gives us the ability to compare measurements among sites. Consequently, the ranking of the slopes may give us new information and will have utility for spatial upscaling of canopy photosynthesis if these relations are to be applied to interpret measurements derived from remote sensing platforms. On hourly and daily time scales, Table 2 shows that the C_4 corn had the steepest slope, as expected, because C_4 plants have a greater quantum efficiency than C_3 plants (Pearcy & Ehleringer, 1984). Quantitatively, the A_c-NIR_v slope of the corn canopy was about 25% greater than that for the C_3 tule/cattail wetland, which was deciduous and harbored a significant fraction of dead legacy vegetation that also intercepted photons. In turn, the A_c-NIR_v slope of the tule/cattails was about 10% less than that of the nitrogen fixing alfalfa. While both are perennial vegetation, the alfalfa experienced repeated cuttings, which altered the amount of light it absorbed. Yet, the relation between A_c and NIR_v remained tight across a wide range in the fraction of absorbed light. The native ecosystems on nitrogen-poorer soils experienced the smallest slopes. Otherwise, the relation between A_c and NIR_v remained tight as the ecosystems experienced a wide range in carbon assimilation due to soil water deficits and temperature stress, instead of cutting.

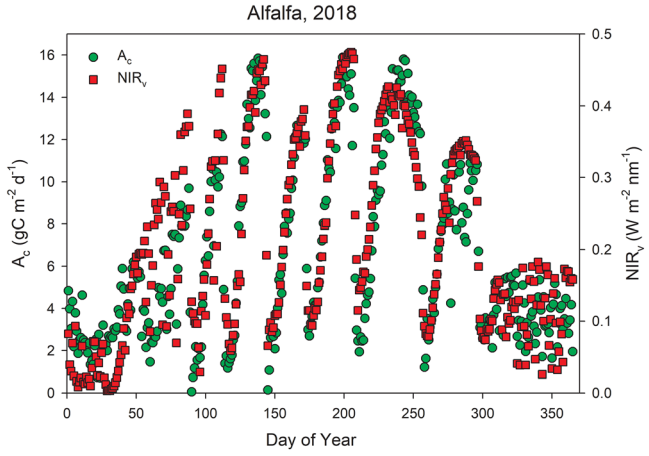

Figure 5. Seasonal patterns of daily integrated canopy photosynthesis (A_c), mean reflected NIR from vegetation (NIR_v), plotted by day over alfalfa across multiple harvest dates. Day of year starts in 2018.

No proxy or reference is perfect. Some of the scatter observed in Figures 2, 4, 6, 8, and 10 can be attributed to sampling error of the eddy covariance measurements (Moncrieff et al., 1996; Richardson et al., 2006), errors in the partitioning of direct measurements of net ecosystem carbon exchange into canopy photosynthesis (Reichstein et al., 2005), and

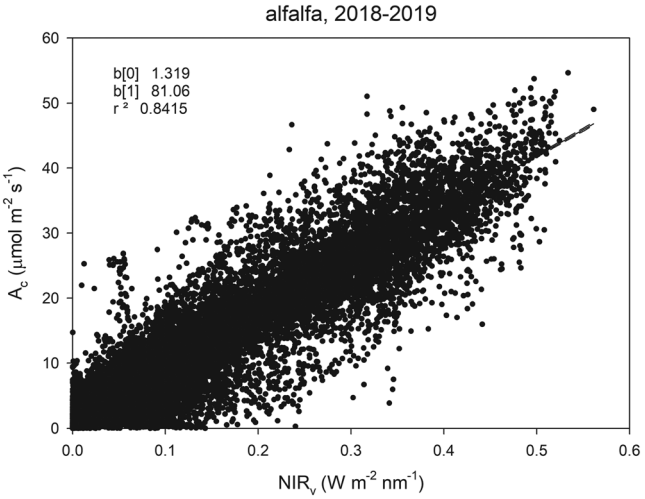

Figure 6. One-to-one plot between canopy photosynthesis of alfalfa and the near-infrared radiation reflected from the vegetation. These data are plotted according to the aerodynamic canopy height. The data are from 2018 and 2019 and are half-hour averages between 0900 and 1700 hours. The slope is 81.1 (μmol m^{-2} s^{-1})/(W m^{-2} nm^{-1}), and the coefficient of determination, r^2, is 0.841.

differences between the relatively large flux footprint (Kljun et al., 2015) and the smaller footprint observed by the light sensors.

4.1. Interannual Variability

If the relation between NIR_v and A_c is to have wider utility, it will need to work across multiple years. In California, interannual variation in spring rain and temperature have a huge effect on annual canopy photosynthesis through the timing of the start and end of the growing season (Ma et al., 2007; Ma et al., 2016), which can vary by up to 50 days (Figure 11). A question that remains begging is whether or not reflected near-infrared radiation from vegetation can serve as a successful proxy for such year-to-year variation in annual canopy photosynthesis.

While we only have up to 3 years of data with the commercial red and NIR sensors, we started measuring reflected red and near-infrared radiation over the annual grassland in 2007 with a homebuilt light-emitting diode sensor (Ryu et al., 2010). While it has different properties from the sensors used in this study, we can extract information from it on the reflected NIR_v. Hence, we can address how well reflected near-infrared radiation from vegetation correlates with A_c for a wide range in rain and growing conditions. Figure 12 shows the comparison between daily integrated canopy photosynthesis and midday NIR_v for 12 years. Year-to-year variability in the slopes was relatively small, being on the order of ±11% (0.044 ± 0.0049 gC m^{-2} day^{-1}/W m^{-2}). Moreover, the coefficient of determination, r^2, on the regression between A_c and NIR_v was high, 0.762, which is nearly as good as the commercial sensor over a shorter time frame. This figure gives us confidence that we may be able to extract information on interannual variation of A_c from measurements of NIR_v from satellite-based sensors.

4.2. Theoretical Basis

On first inspection it may seem counterintuitive how and why ecosystem photosynthesis would be related so closely to reflected near-infrared radiation from vegetation. However, we can make a case based on its relation to absorbed sunlight and its superiority to light use efficiency models.

Dechant et al. (2020) recently showed that over 50% to 80% of the variance in A_c was explained in terms of the product absorbed visible light times the fraction of photons escaping the canopy, f_{esc}.

$$A_c = Q_{a,P} \cdot f_{esc} \quad (1)$$

In comparison they found that the classic light use efficiency equation explained only 40% to 50% of the variance in A_c.

Why does this occur? Zeng et al. (2019)) showed that the fraction of photons escaping the canopy, f_{esc}, is defined as the ratio of the reflectance of near-infrared radiation from the vegetation (ρ_{NIRv}) and the fraction of absorbed photosynthetically active radiation, $f_{a,P}$.

$$f_{esc} = \frac{\rho_{NIR_v}}{f_{a,P}} \quad (2)$$

Traditionally, A_c has been computed from space as a function of photon flux density of photosynthetically active quanta absorbed by green vegetation ($Q_{a,P}$) times a light use efficiency (ϕ),

$$A_c = Q_{a,P} \cdot \phi \quad (3)$$

In equation 3, $Q_{a,P}$ is the product of fraction of absorbed photosynthetically active quanta ($f_{a,P}$) times the photon flux density of incident photosynthetically active quanta, Q_P:

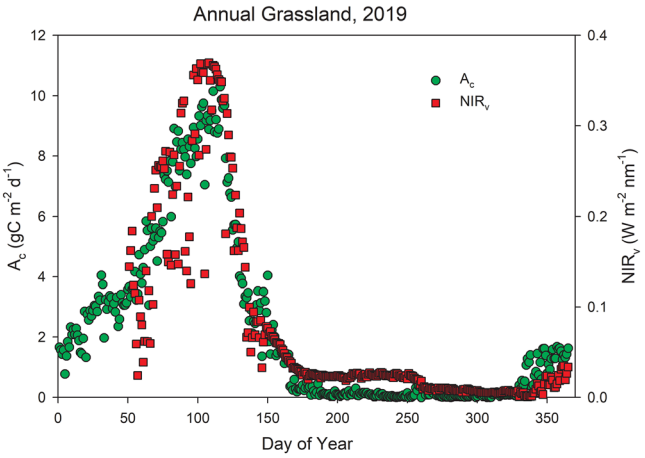

Figure 7. Seasonal patterns of canopy photosynthesis (A_c), mean reflected NIR from vegetation (NIR_V) over an annual grassland. Day of year starts in 2019.

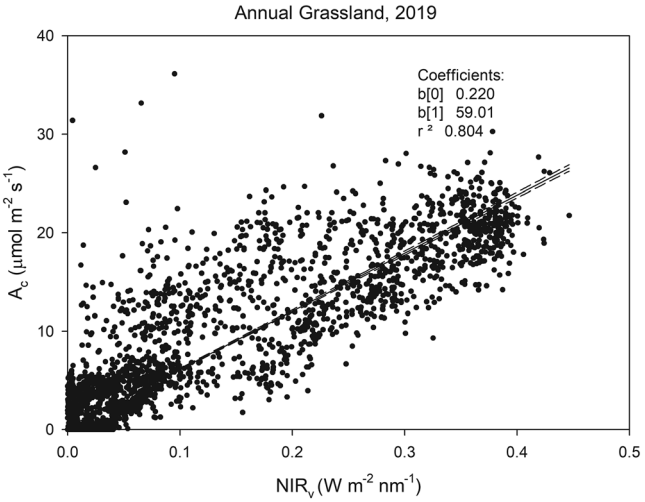

Figure 8. Plot between canopy photosynthesis, A_c, and NIR_V. Data are half-hour averages between 1000 and 1600 hours, from 2019.

$$Q_{a,P} = f_{a,P} \cdot Q_P \quad (4)$$

Thereby, $f_{a,P}$ is defined as

$$f_{a,P} = \frac{Q_{a,P}}{Q_P} \quad (5)$$

With further algebraic manipulation we can define A_c as a function of the reflectance of NIR from vegetation (ρ_{NIRv}), which scales with the flux density of near-infrared radiation reflected by vegetation, NIR_V.

$$A_c = Q_{a,P} \cdot f_{esc} = f_{a,P} \cdot Q_P \frac{\rho_{NIR_V}}{f_{a,P}} = Q_P \cdot \rho_{NIR_V} \sim NIR_V \quad (6)$$

The identity $Q_P \cdot \rho_{NIR_V} \sim NIR_V$ holds because incoming solar radiation is about half visible and half near infrared (Ross, 1980), so it is legitimate to substitute Q_P with incoming NIR. Together, this set of equations provide a theoretical explanation for the empirical results we show in the paper.

4.3. Interpreting Field Measurements With the CanVeg Model

To better understand how structure and function influence the relation we observed between A_c and NIR_V, we ran simulations of the biophysical CanVeg model. We used the conditions for an alfalfa field, which was tested and validated in an earlier paper (Oikawa et al., 2017). We compared computations of canopy photosynthesis with computations of broadband NIR reflected from the vegetation for the cases when soil reflectance was 0.

First, we ran simulations for a range of leaf area indices. Figure 13 shows a strong theoretical and linear relation between the two variables, which is consistent with the linearity of the results shown above; in general, r^2 values are very high ($r^2 > 0.94$). Theoretically, there is overlap between A_c and NIR_V for a family of leaf area indices; technically, the slopes ranged between 0.117 and 0.133) with increasing leaf area indices (1 to 4). And it is noteworthy that the relationship between these two variables does not saturate at high reflectance values or low leaf area indices, as NDVI may do (Sellers, 1985). From these calculations, we conclude that the differences in slopes observed over the tules/cattails and alfalfa were not due to differences in leaf area index. This relative invariance with leaf area index helps explain why this correlation held well over the alfalfa crop that experienced multiple cuttings.

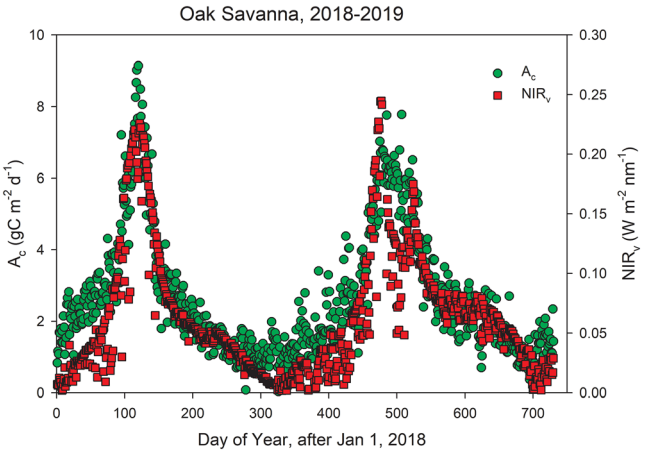

Figure 9. Seasonal patterns of daily integrated canopy photosynthesis (A_c) and mean reflected NIR from vegetation (NIR_V), plotted by day over oak savanna. Day of year starts in 2018 and runs through 2019.

Leaf photosynthesis models depend upon the specification of the maximum carboxylation velocity (V_{cmax}) (Farquhar et al., 1980), a measure of photosynthetic capacity. We hypothesize that the ranking among C_3 canopies may be associated with differences in soil nitrogen, which affects leaf nitrogen and photosynthetic capacity.

We base this hypothesis on the connected evidence that photosynthetic capacity (Field & Mooney, 1986) and the amount of reflected near-infrared radiation by a canopy (Ollinger, 2011; Ollinger et al., 2008) scales with nitrogen. If true, this conjecture would be consistent with the observation that greater values in canopy photosynthesis were associated with greater flux densities of reflected near-infrared radiation, and vice versa. There remains controversy as to the mechanism explaining the correlation between reflected NIR and leaf nitrogen because nutrition can affect canopy structure and plant traits, which also influence canopy near-infrared radiation reflectance (Knyazikhin et al., 2013; Ollinger et al., 2013).

To explore the hypothesis that the slope between A_c and NIR_V depended upon photosynthetic capacity, we ran the CanVeg model and changed

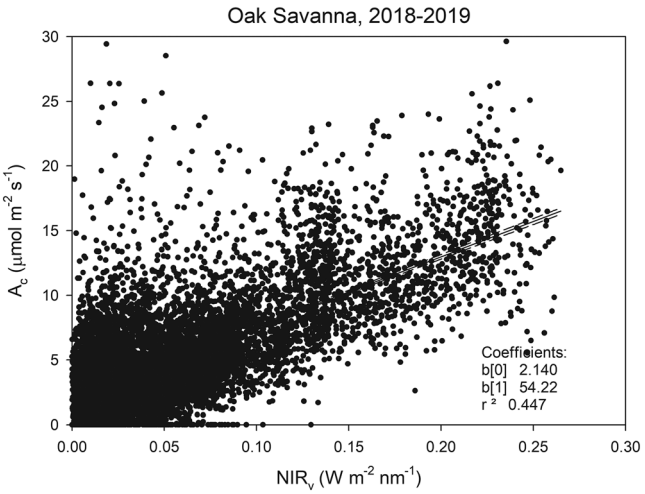

Figure 10. One-to-one plot between canopy photosynthesis of oak savanna and the near-infrared radiation reflected from the vegetation. The data are from 2018 and 2019.

the relative fraction of maximum carboxylation velocity (V_{cmax}) as a proxy for changing leaf nitrogen. Figure 14 shows that we get a family of curves between A_c and NIR_v, with gradually flattening slopes as V_{cmax} decreases. As V_{cmax} decreased by 20% to 40%, the slope between A_c and NIR_v dropped by 10% to 21%. These results are consistent with recent computations that showed that Sun-induced fluorescence, which scales with NIR_v, decreased with decreasing V_{cmax} (Qiu et al., 2019). In sum, these computations tie together the connections between photosynthetic rates, leaf nitrogen, photosynthetic capacity, and the amount of NIR reflected from leaves and canopies, discussed above.

Canopy photosynthesis is known to increase with increasing diffuse fraction at a given light level. Why? As the sky becomes more isotropic, photons are better trapped by the vegetation, shaded leaves receive more sunlight, and sunlit leaves receive less sunlight. Together, these interactions increase canopy photosynthesis for a given level of incoming sunlight by increasing integrated canopy light use efficiency and by increasing the canopy's ability to absorb light (Jarvis et al., 1985; Knohl & Baldocchi, 2008; Niyogi et al., 2004).

To test this hypothesis, we applied the CanVeg model to examine the effect of diffuse light during the 2018 smoke period that veiled California in 2018 (Hemes et al., 2020). Like the field measurements, the model computations indicate that a steeper slope between A_c and NIR_v occurs when diffuse light fraction is greater (Figure 15). As noted above, diffuse light coming into the canopy from multiple angles is trapped better and is converted into photosynthesis more efficiently. In these circumstances, diffuse conditions alter canopy photosynthesis but has no immediate effect on canopy structure, as proxied by NIR_v, resulting in a transient deviation in the mean NIR_v-A_c relationship. The results here confirm the empirical findings reported for the corn, tule/cattails, and alfalfa.

4.4. Relation to Past Work

The late Piers Seller (Sellers, 1987; Sellers et al., 1992) proposed that the photosynthesis of a vegetated canopy should be a linear function of the flux density of near-infrared photons reflected from that canopy. The proposition was based on the conjecture that reflected near-infrared radiation is a proxy for the fraction of visible light absorbed by the canopy (f_{QP}). Why and how? In principle, Sellers argues that the change in NIR reflectance from vegetation (ρ_{NIRv}) with a change in leaf area index (L) is proportional to the change in the fraction of absorbed Q_P with leaf area index, $f_{a,P}$:

$$\frac{d\rho_{nir}}{dL} \sim \frac{df_{a,P}}{dL} \quad (7)$$

Incoming photons in the visible and near-infrared wave bands have the same probability of passing through gaps in the canopy and intercepting leaves. It is how these photons, with different wavelengths, interact with leaves and exit the canopy that differ, as the scattering coefficient of near-infrared radiation is much greater than that of visible radiation. Sellers et al. (1992) explains this behavior by the following:

"... near infrared reflectance is proportional to double the pathlength of near infrared radiation in the canopy as this radiation must enter and leave the canopy, while $f_{a,P}$ is proportional to only the one-way penetration ...."

To test this conjecture, we computed the reflectance of near-infrared radiation from the vegetation (ρ_{NIRv}) and $f_{a,P}$ as a function of leaf area

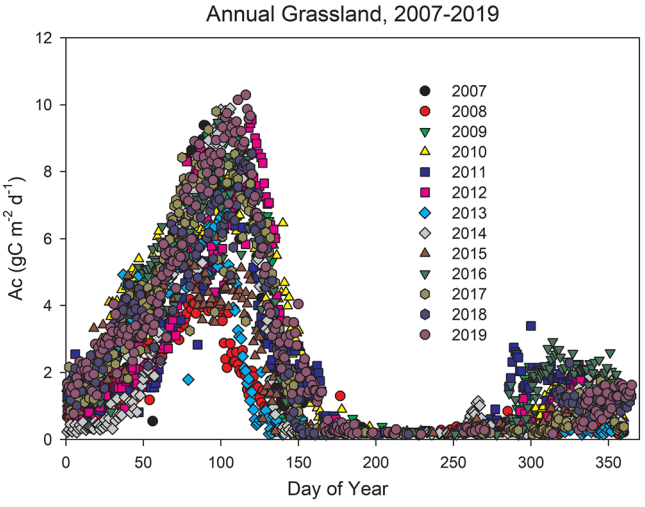

Figure 11. Interannual variability of daily integrated canopy photosynthesis over the annual grassland between 2007 and through 2019.

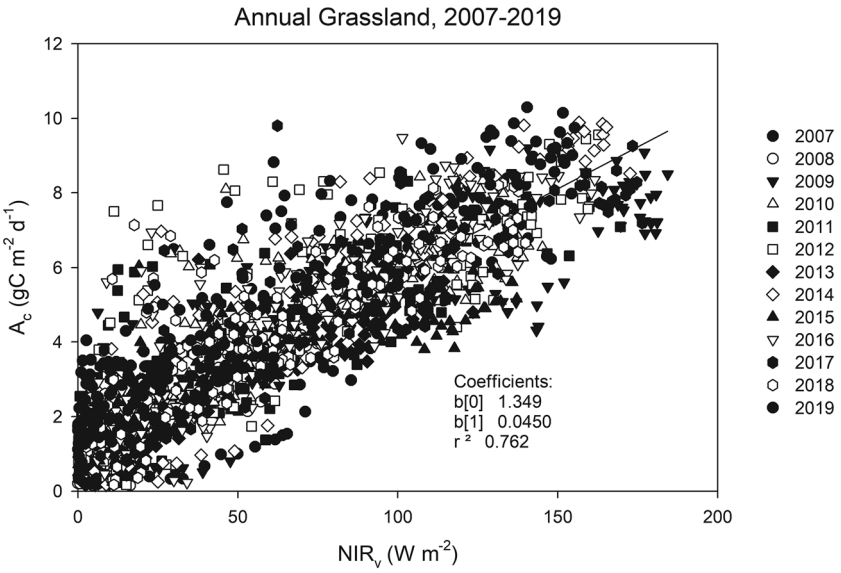

Figure 12. Correlation between ecosystem photosynthesis of an annual grassland and reflected near-infrared radiation from vegetation. These data are for the 2007 through 2019 time frame and are based on a homebuilt light-emitting diode sensor. The coefficient of determination, r^2, was 0.762 over these 12 years.

index, L. Figure 16 shows that the relative change in ρ_{NIRv} with L is similar to the relative change in $f_{\mathrm{a,P}}$ with L, lending support to the Sellers conjecture in equation 5.

How absorbed visible, or reflected near-infrared, radiation leads to a linear dependence by photosynthesis arises from ecophysiological optimality. Under optimal conditions, plants invest just enough nitrogen such that the mean light environment, which decreases exponentially with cumulative leaf area index, is close to

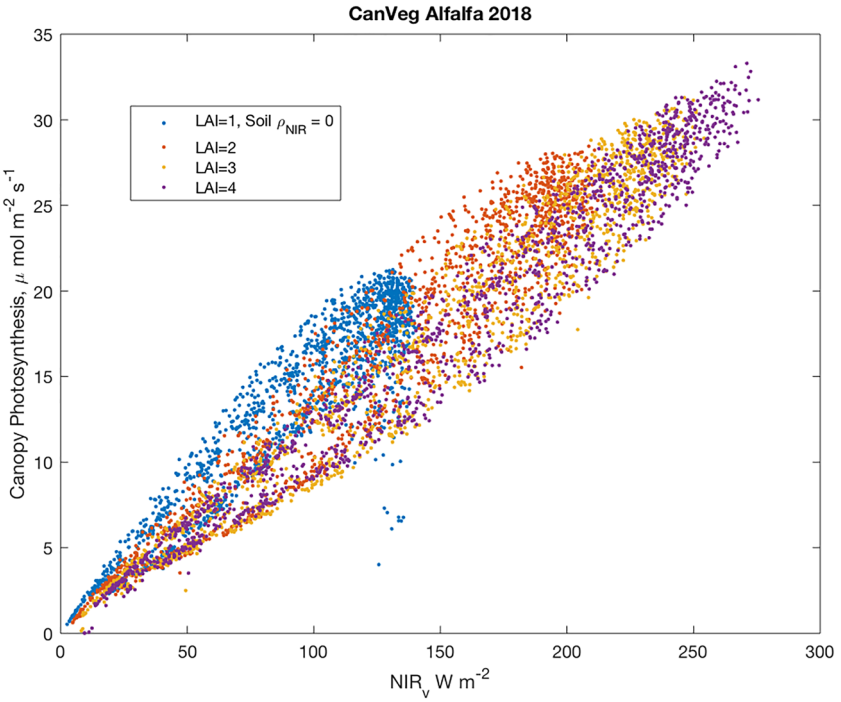

Figure 13. Simulations of canopy photosynthesis and reflected near-infrared radiation. The computations were run for a range of leaf area index. The model assumed the structure and function of an alfalfa canopy. Data are reported for when leaf temperature was less than 28°C. Meteorological inputs were from the summer of 2018.

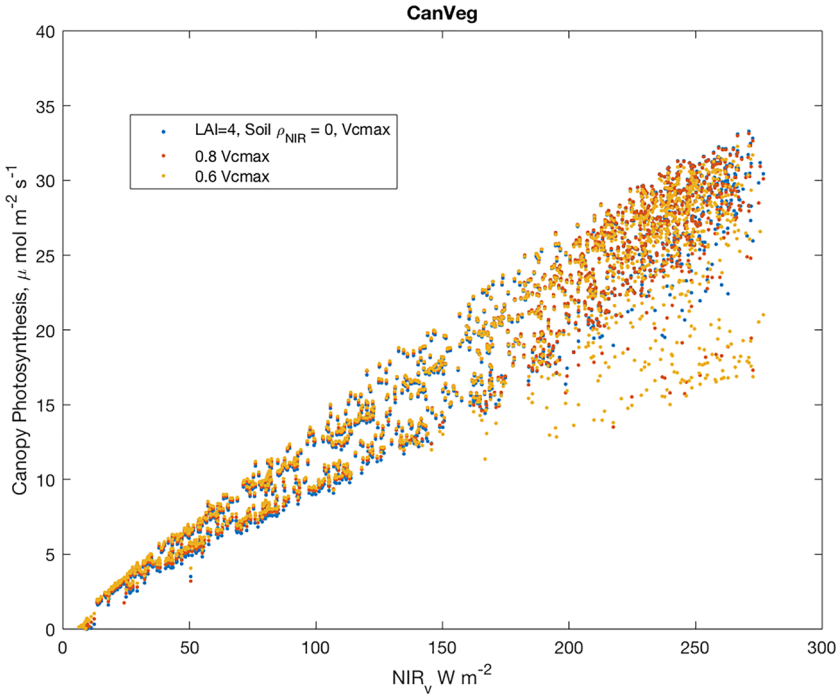

Figure 14. Computations of canopy photosynthesis and reflected near-infrared radiation from vegetation. Runs were performed for a closed canopy (LAI = 4) and a range of maximum carboxylation capacity of the leaf photosynthesis model; the reference value of V_{cmax} was 170 μmol m^{-2} s^{-1}.

the inflection point between light saturation and light dependence (Anten, 2016; Hikosaka, 2014; Hikosaka & Terashima, 1995; Hirose & Werger, 1987). By having photosynthetic capacity, as defined by nitrogen content per unit area, decrease with depth in the canopy, the integration of leaf photosynthesis layer by layer produces a linear response between canopy photosynthesis and absorbed visible light (Sellers et al., 1992).

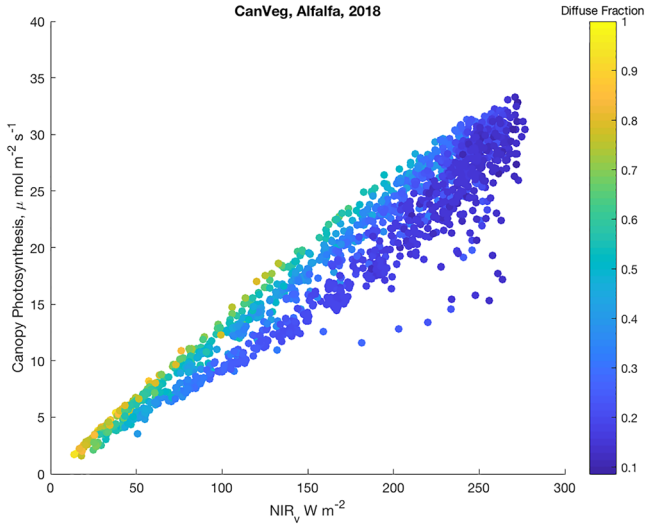

Figure 15. Computations of canopy photosynthesis and near-infrared radiation reflected by vegetation, as a function of diffuse light fraction. Computations were confined to periods with low vapor pressure deficits. Computations were based on half-hour meteorological data from between Days 195 and 258 in 2018 when smoke from fires in northern California veiled the ecosystems.

4.5. Further Directions

In the past decade there has been a growing number of papers inferring ecosystem photosynthesis to the global scale from measurements of Sun-induced fluorescence (Frankenberg et al., 2014; Guan et al., 2015; Guanter et al., 2013; Meroni et al., 2009; Parazoo et al., 2014; Porcar-Castell et al., 2014). Although Sun-induced fluorescence is gaining much popularity, it faces many technical challenges before it can be used widely to assess ecosystem photosynthesis. First, Sun-induced fluorescence has narrow emission peaks (near 680 and 740 nm) and the photon flux density leaving the canopy is tiny compared to the background signal of reflected radiation (Guanter et al., 2013; Meroni et al., 2009; Porcar-Castell et al., 2014). These constraints require a spectroradiometer with very high spectral resolution and high signal-to-noise ratio (Damm et al., 2011; Meroni et al., 2009). Second, the amount of solar-induced fluorescence observed by a satellite or a tower-mounted spectrometer consists of three mechanistic components. These components are the amount of absorbed radiation, the physiological fluorescence emission yield, and the fraction of photons that escape the canopy (Gu et al., 2019; van der Tol, Verhoef, & Rosema, 2009; van der Tol, Verhoef, Timmermans, et al., 2009; Yang & van der Tol, 2018; Zeng et al., 2019). The interpretation of solar-induced fluorescence requires better information on (1) how canopy structure (e.g., leaf area index, leaf angle, and leaf clumping) affects the absorption of solar radiation; (2) sensitivity of fluorescence

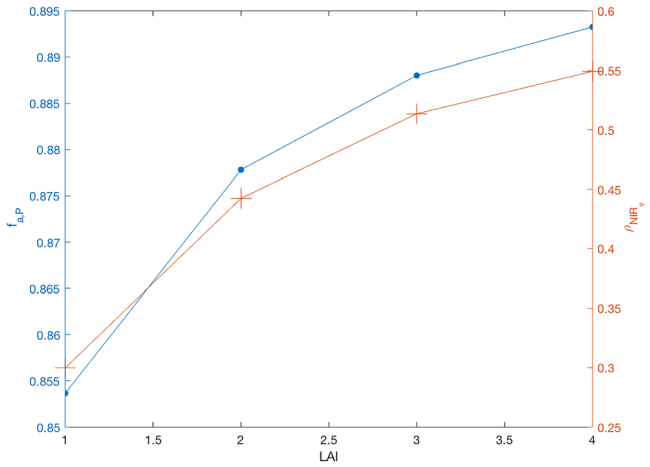

Figure 16. Sensitivity of the fraction of absorbed quantum flux density of visible light (left axis) or near-infrared reflectance (right axis) with leaf area index, *L*.

production to photosynthetic capacity (Verma et al., 2017), which may vary with leaf nutrition or physiological stress; and (3) how fluorescent photons escape the canopy through a tortuous path of gaps and multiple scattering (Qiu et al., 2019; Zeng et al., 2019).

There is growing evidence that solar-induced fluorescence escaping the canopy may better represent the amount of visible light absorbed by green vegetation (Badgley et al., 2017; Yang et al., 2018) rather than being a correlate with canopy photosynthesis, per se. Therefore, if solar-induced fluorescence escaping the canopy is just a measure of absorbed light, are there easier and more direct ways to measure absorbed light, in order to assess canopy photosynthesis? Here we provide direct evidence of the power of using NIR_V, instead, especially given its stronger signal and its history being measured on many satellites for decades. Of course, many pertinent questions remain. For example, how to upscale single observations from space to daily integrals (Sims et al., 2005).

The key aspect of applying measured reflected NIR from vegetation as a proxy to canopy photosynthesis is to remove signal contaminated by soil and dead vegetation. At present, NIR_V is determined by measuring reflected NIR times a renormalized NDVI that ranges between 0 and 1. More work is needed to test the universality of this assumption, especially for sparse canopies that do not achieve a high NDVI value, near 1.

5. Conclusions

Reflected near-infrared radiation from green vegetation was found to be a strong predictor of canopy photosynthesis on across hourly, daily, seasonal, and interannual time scales. This simple and inexpensive measure also worked well across a wide range of structural and functional types and weather conditions.

This paper raises the potential to use this simpler and inexpensive vegetation metric to scale photosynthesis more widely. For example, information on reflected near-infrared radiation from vegetation may have utility in monitoring carbon assimilation in carbon sequestration projects or on microsatellites orbiting Earth for precision agriculture applications. And it does not suffer from many of the idiosyncrasies associated with the measurement and interpretation of NDVI or Sun-induced fluorescence. We recommend that more eddy covariance flux towers add this set of measurements.

Acknowledgments

This research was supported by contracts from the California Department of Fish and Wildlife and Water Resources and the Department of Energy, Office of Science, through the AmeriFlux project. Y. R. and B. D. were supported by the National Research Foundation of Korea (NRF-2016M1A3A3A02018195). D. D. B.'s visit to Y. R.'s lab was supported by Prestigious Foreign Scholar Program by Seoul National University. In compliance with the AGU FAIR data policy, our data are submitted to the Ameriflux database, where they are available to all (https://ameriflux.lbl.gov/data/download-data/).

References

Anten, N. P. R. (2016). Optimization and game theory in canopy models. In K. Hikosaka, Ü. Niinemets, & N. P. R. Anten (Eds.), *Canopy photosynthesis: From basics to applications*, (pp. 355–377). Dordrecht: Springer Netherlands. https://doi.org/10.1007/978-94-017-7291-4_13

Aragon, B., Houborg, R., Tu, K., Fisher, J. B., & McCabe, M. (2018). CubeSats enable high spatiotemporal retrievals of crop-water use for precision agriculture. *Remote Sensing*, *10*(12), 1867.

Badgley, G., Anderegg, L. D. L., Berry, J. A., & Field, C. B. (2019). Terrestrial gross primary production: Using NIRV to scale from site to globe. *Global Change Biology*, *25*(11), 3731–3740. https://doi.org/10.1111/gcb.14729

Badgley, G., Field, C. B., & Berry, J. A. (2017). Canopy near-infrared reflectance and terrestrial photosynthesis. *Science Advances*, *3*(3).

Baldocchi, D. D. (2003). Assessing the eddy covariance technique for evaluating carbon dioxide exchange rates of ecosystems: Past, present and future. *Global Change Biology*, *9*, 479–492.

Baldocchi, D. D., Fuentes, J., Bowling, D., Turnipseed, A., & Monson, R. (1999). Scaling isoprene fluxes from leaves to canopies: Test cases over a boreal aspen and a mixed temperate forest. *Journal of Applied Meteorology*, *38*, 885–898.

Baldocchi, D. D., & Meyers, T. (1998). On using eco-physiological, micrometeorological and biogeochemical theory to evaluate carbon dioxide, water vapor and trace gas fluxes over vegetation: A perspective. *Agricultural and Forest Meteorology*, *90*(1–2), 1–25.

Baldocchi, D. D., Xu, L., & Kiang, N. (2004). How plant functional-type, weather, seasonal drought, and soil physical properties alter water and energy fluxes of an oak-grass savanna and an annual grassland. *Agricultural and Forest Meteorology*, *123*(1–2), 13–39.

Béland, M., Baldocchi, D. D., Widlowski, J.-L., Fournier, R. A., & Verstraete, M. M. (2014). On seeing the wood from the leaves and the role of voxel size in determining leaf area distribution of forests with terrestrial LiDAR. *Agricultural and Forest Meteorology*, *184*, 82–97. https://doi.org/10.1016/j.agrformet.2013.09.005

Bonan, G. B., & Doney, S. C. (2018). Climate, ecosystems, and planetary futures: The challenge to predict life in Earth system models. *Science*, *359*(6375).

Canadell, J. G., Mooney, H. A., Baldocchi, D. D., Berry, J. A., Ehleringer, J. R., Field, C. B., et al. (2000). Commentary: Carbon metabolism of the terrestrial biosphere: A multitechnique approach for improved understanding. *Ecosystems*, *3*(2), 115–130. https://doi.org/10.1007/s100210000014

Chen, Q., Gong, P., Baldocchi, D., & Tian, Y. Q. (2007). Estimating basal area and stem volume for individual trees from lidar data. *Photogrammetric Engineering and Remote Sensing*, *73*(12), 1355–1365.

Chu, H., Baldocchi, D. D., Poindexter, C., Abraha, M., Desai, A. R., Bohrer, G., et al. (2018). Temporal dynamics of aerodynamic canopy height derived from eddy covariance momentum flux data across North American Flux Networks. *Geophysical Research Letters*, *45*, 9275–9287. https://doi.org/10.1029/2018GL079306

Collatz, G. J., Ball, J. T., Grivet, C., & Berry, J. A. (1991). Physiological and environmental regulation of stomatal conductance, photosynthesis and transpiration: A model that includes a laminar boundary layer. *Agricultural and Forest Meteorology*, *54*(2–4), 107–136.

Damm, A., Erler, A., Hillen, W., Meroni, M., Schaepman, M. E., Verhoef, W., & Rascher, U. (2011). Modeling the impact of spectral sensor configurations on the FLD retrieval accuracy of Sun-induced chlorophyll fluorescence. *Remote Sensing of Environment*, *115*(8), 1882–1892. https://doi.org/10.1016/j.rse.2011.03.011

Dechant, B., Ryu, Y., Badgley, G., Zeng, Y., Berry, J. A., Zhang, Y., et al. (2020). Canopy structure explains the relationship between photosynthesis and Sun-induced chlorophyll fluorescence in crops. *Remote Sensing of Environment*, *241*, 111733. https://doi.org/10.1016/j.rse.2020.111733

Detto, M., Verfaillie, J., Anderson, F., Xu, L., & Baldocchi, D. (2011). Comparing laser-based open- and closed-path gas analyzers to measure methane fluxes using the eddy covariance method. *Agricultural and Forest Meteorology*, *151*(10), 1312–1324. https://doi.org/10.1016/j.agrformet.2011.05.014

Dronova, I., & Taddeo, S. (2016). Canopy leaf area index in non-forested marshes of the California Delta. *Wetlands*, *36*(4), 705–716. https://doi.org/10.1007/s13157-016-0780-5

Eichelmann, E., Hemes, K. S., Knox, S. H., Oikawa, P. Y., Chamberlain, S. D., Sturtevant, C., et al. (2018). The effect of land cover type and structure on evapotranspiration from agricultural and wetland sites in the Sacramento–San Joaquin River Delta, California. *Agricultural and Forest Meteorology*, *256–257*, 179–195. https://doi.org/10.1016/j.agrformet.2018.03.007

Eichelmann, E., Wagner-Riddle, C., Warland, J., Deen, B., & Voroney, P. (2016). Evapotranspiration, water use efficiency, and energy partitioning of a mature switchgrass stand. *Agricultural and Forest Meteorology*, *217*, 108–119. https://doi.org/10.1016/j.agrformet.2015.11.008

Falge, E., Baldocchi, D., Tenhunen, J., Aubinet, M., Bakwin, P., Berbigier, P., et al. (2002). Seasonality of ecosystem respiration and gross primary production as derived from FLUXNET measurements. *Agricultural and Forest Meteorology*, *113*(1–4), 53–74.

Farquhar, G. D., Caemmerer, S. V., & Berry, J. A. (1980). A biochemical-model of photosynthetic CO_2 assimilation in leaves of C-3 species. *Planta*, *149*(1), 78–90.

Field, C. H., & Mooney, H. A. (1986). Photosynthesis-nitrogen relationship in wild plants. In *On the Economy of Plant Form and Function: Proceedings of the Sixth Maria Moors Cabot Symposium, Evolutionary Constraints on Primary Productivity, Adaptive Patterns of Energy Capture in Plants, Harvard Forest, August 1983*. Cambridge [Cambridgeshire]: Cambridge University Press.

Field, C. B., Randerson, J. T., & Malmstrom, C. M. (1995). Global net primary production: Combining ecology and remote sensing. *Remote Sensing of Environment*, *51*(1), 74–88.

Frankenberg, C., O'Dell, C., Berry, J., Guanter, L., Joiner, J., Kohler, P., et al. (2014). Prospects for chlorophyll fluorescence remote sensing from the Orbiting Carbon Observatory-2. *Remote Sensing of Environment*, *147*, 1–12. https://doi.org/10.1016/j.rse.2014.02.007

Griscom, B. W., Adams, J., Ellis, P. W., Houghton, R. A., Lomax, G., Miteva, D. A., et al. (2017). Natural climate solutions. *Proceedings of the National Academy of Sciences*, *114*(44), 11645–11650. https://doi.org/10.1073/pnas.1710465114

Gu, L., Han, J., Wood, J. D., Chang, C. Y.-Y., & Sun, Y. (2019). Sun-induced Chl fluorescence and its importance for biophysical modeling of photosynthesis based on light reactions. *New Phytologist*, *223*, 1179–1191. https://doi.org/10.1111/nph.15796

Guan, K., Berry, J. A., Zhang, Y., Joiner, J., Guanter, L., Badgley, G., & Lobell, D. B. (2015). Improving the monitoring of crop productivity using spaceborne solar-induced fluorescence. *Global Change Biology*, *22*(2), 716–726. https://doi.org/10.1111/gcb.13136

Guanter, L., Rossini, M., Colombo, R., Meroni, M., Frankenberg, C., Lee, J.-E., & Joiner, J. (2013). Using field spectroscopy to assess the potential of statistical approaches for the retrieval of Sun-induced chlorophyll fluorescence from ground and space. *Remote Sensing of Environment*, *133*, 52–61. https://doi.org/10.1016/j.rse.2013.01.017

Heinsch, F. A., Zhao, M., Running, S. W., Kimball, J. S., Nemani, R. R., Davis, K. J., et al. (2006). Evaluation of remote sensing based terrestrial productivity from MODIS using regional tower Eddy flux network observations. *Geoscience and Remote Sensing, IEEE Transactions on*, *44*(7), 1908–1925. https://doi.org/10.1109/TGRS.2005.853936

Hemes, K. S., Chamberlain, S. D., Eichelmann, E., Anthony, T., Valach, A., Kasak, K., et al. (2019). Assessing the carbon and climate benefit of restoring degraded agricultural peat soils to managed wetlands. *Agricultural and Forest Meteorology*, *268*, 202–214. https://doi.org/10.1016/j.agrformet.2019.01.017

Hemes, K. S., Verfaillie, J., & Baldocchi, D. D. (2020). Wildfire-smoke aerosols lead to increased light use efficiency among agricultural and restored wetland land uses in California's Central Valley. *Journal of Geophysical Research: Biogeosciences*, *125*, e2019JG005380. https://doi.org/10.1029/2019JG005380

Hikosaka, K. (2014). Optimal nitrogen distribution within a leaf canopy under direct and diffuse light. *Plant, Cell & Environment*, *37*(9), 2077–2085. https://doi.org/10.1111/pce.12291

Hikosaka, K., & Terashima, I. (1995). A model of the acclimation of photosynthesis in the leaves of C3 plants to Sun and shade with respect to nitrogen use. *Plant, Cell & Environment*, *18*(6), 605–618. https://doi.org/10.1111/j.1365-3040.1995.tb00562.x

Hirose, T., & Werger, M. J. A. (1987). Nitrogen use efficiency in instantaneous and daily photosynthesis of leaves in the canopy of a *Solidago altissima* stand. *Physiologia Plantarum*, *70*(2), 215–222. https://doi.org/10.1111/j.1399-3054.1987.tb06134.x

Jarvis, P. G., Miranda, H. S., & Muetzelfeldt, R. I. (1985). Modelling canopy exchanges of water vapor and carbon dioxide in coniferous forest plantations. In B. A. Hutchison, & B. B. Hicks (Eds.), *The forest-atmosphere interaction: Proceedings of the Forest Environmental Measurements Conference held at Oak Ridge, Tennessee, October 23–28, 1983*, (pp. 521–542). Dordrecht: Springer Netherlands. https://doi.org/10.1007/978-94-009-5305-5_31

Kim, J., Guo, Q., Baldocchi, D., Leclerc, M., Xu, L., & Schmid, H. (2006). Upscaling fluxes from tower to landscape: Overlaying flux footprints on high-resolution (IKONOS) images of vegetation cover. *Agricultural and Forest Meteorology*, *136*(3–4), 132–146. https://doi.org/10.1016/j.agrformet.2004.11.015

Kljun, N., Calanca, P., Rotach, M. W., & Schmid, H. P. (2015). A simple two-dimensional parameterisation for flux footprint prediction (FFP). *Geoscientific Model Development*, *8*(11), 3695–3713. https://doi.org/10.5194/gmd-8-3695-2015

Knohl, A., & Baldocchi, D. D. (2008). Effects of diffuse radiation on canopy gas exchange processes in a forest ecosystem. *Journal of Geophysical Research*, *113*, G02023. https://doi.org/10.1029/2007JG000663

Knox, S. H., Sturtevant, C., Matthes, J. H., Koteen, L., Verfaillie, J., & Baldocchi, D. (2015). Agricultural peatland restoration: Effects of land-use change on greenhouse gas (CO_2 and CH_4) fluxes in the Sacramento-San Joaquin Delta. *Global Change Biology*, *21*(2), 750–765. https://doi.org/10.1111/gcb.12745

Knyazikhin, Y., Schull, M. A., Stenberg, P., Mõttus, M., Rautiainen, M., Yang, Y., et al. (2013). Hyperspectral remote sensing of foliar nitrogen content. *Proceedings of the National Academy of Sciences of the United States of America*, *110*(3), E185–E192. https://doi.org/10.1073/pnas.1210196109

Ma, S., Baldocchi, D., Wolf, S., & Verfaillie, J. (2016). Slow ecosystem responses conditionally regulate annual carbon balance over 15 years in Californian oak-grass savanna. *Agricultural and Forest Meteorology*, *228*, 252–264. https://doi.org/10.1016/j.agrformet.2016.07.016

Ma, S., Baldocchi, D. D., Xu, L., & Hehn, T. (2007). Inter-annual variability in carbon dioxide exchange of an oak/grass savanna and open grassland in California. *Agricultural and Forest Meteorology*, *147*(3–4), 157–171. https://doi.org/10.1016/j.agrformet.2007.07.008

Meroni, M., Rossini, M., Guanter, L., Alonso, L., Rascher, U., Colombo, R., & Moreno, J. (2009). Remote sensing of solar-induced chlorophyll fluorescence: Review of methods and applications. *Remote Sensing of Environment*, *113*(10), 2037–2051. https://doi.org/10.1016/j.rse.2009.05.003

Michalsky, J. J., Berndt, J. L., & Schuster, G. J. (1986). A microprocessor-based rotating shadowband radiometer. *Solar Energy*, *36*(5), 465–470.

Moffat, A. M., Papale, D., Reichstein, M., Hollinger, D. Y., Richardson, A. D., Barr, A. G., et al. (2007). Comprehensive comparison of gap-filling techniques for eddy covariance net carbon fluxes. *Agricultural and Forest Meteorology*, *147*(3–4), 209–232. https://doi.org/10.1016/j.agrformet.2007.08.011

Moncrieff, J., Malhi, Y., & Leuning, R. (1996). The propogation of errors in long-term measurements of carbon and water. *Global Change Biology*, *2*, 231–240.

Niyogi, D., Chang, H. I., Saxena, V. K., Holt, T., Alapaty, K., Booker, F., et al. (2004). Direct observations of the effects of aerosol loading on net ecosystem CO_2 exchanges over different landscapes. *Geophysical Research Letters*, *31*, L20506. https://doi.org/10.1029/2004GL020915

Norman, J. M. (1979). Modeling the complete crop canopy. In B. J. Barfield, & J. F. Gerber (Eds.), *Modification of the aerial environment of plants*, (pp. 249–277). St. Joseph, MI: American Society of Agricultural Engineering.

Norman, J. M. (1981). Interfacing leaf and canopy light interception models. In J. D. Hesketh, & J. W. Jones (Eds.), *Predicting photosynthesis for ecosystem models*, (pp. 49–67). Boca Raton, FL: CRC Press.

Oikawa, P. Y., Sturtevant, C., Knox, S. H., Verfaillie, J., Huang, Y. W., & Baldocchi, D. D. (2017). Revisiting the partitioning of net ecosystem exchange of CO_2 into photosynthesis and respiration with simultaneous flux measurements of $13CO_2$ and CO_2, soil respiration and a biophysical model, CANVEG. *Agricultural and Forest Meteorology*, *234–235*, 149–163.

Ollinger, S. V. (2011). Sources of variability in canopy reflectance and the convergent properties of plants. *The New Phytologist*, *189*(2), 375–394. https://doi.org/10.1111/j.1469-8137.2010.03536.x

Ollinger, S. V., Reich, P. B., Frolking, S., Lepine, L. C., Hollinger, D. Y., & Richardson, A. D. (2013). Nitrogen cycling, forest canopy reflectance, and emergent properties of ecosystems. *Proceedings of the National Academy of Sciences*, *110*(27), E2437. https://doi.org/10.1073/pnas.1304176110

Ollinger, S. V., Richardson, A. D., Martin, M. E., Hollinger, D. Y., Frolking, S. E., Reich, P. B., et al. (2008). Canopy nitrogen, carbon assimilation, and albedo in temperate and boreal forests: Functional relations and potential climate feedbacks. *Proceedings of the National Academy of Sciences of the United States of America*, *105*(49), 19336–19341. https://doi.org/10.1073/pnas.0810021105

Osuna, J. L., Baldocchi, D. D., Kobayashi, H., & Dawson, T. E. (2015). Seasonal trends in photosynthesis and electron transport during the Mediterranean summer drought in leaves of deciduous oaks. *Tree Physiology*. https://doi.org/10.1093/treephys/tpv023

Parazoo, N. C., Bowman, K., Fisher, J. B., Frankenberg, C., Jones, D. B. A., Cescatti, A., et al. (2014). Terrestrial gross primary production inferred from satellite fluorescence and vegetation models. *Global Change Biology*, *20*(10), 3103–3121. https://doi.org/10.1111/gcb.12652

Paw U. K. T., & Gao, W. (1988), Applications of solutions to non-linear energy budget equations, *Agricultural and Forest Meteorology*, *43*, 121–145.

Pearcy, R. W., & Ehleringer, J. (1984). Comparative ecophysiology of C-3 and C-4 plants. *Plant Cell and Environment*, *7*(1), 1–13.

Pennypacker, S., & Baldocchi, D. (2015). Seeing the fields and forests: Application of surface-layer theory and flux-tower data to calculating vegetation canopy height. *Boundary-Layer Meteorology*, *158*(2), 165–182. https://doi.org/10.1007/s10546-015-0090-0

Porcar-Castell, A., Tyystjarvi, E., Atherton, J., van der Tol, C., Flexas, J., Pfundel, E. E., et al. (2014). Linking chlorophyll a fluorescence to photosynthesis for remote sensing applications: Mechanisms and challenges. *Journal of Experimental Botany*, *65*(15), 4065–4095. https://doi.org/10.1093/jxb/eru191

Prentice, I. C., Heimann, M., & Sitch, S. (2000). The carbon balance of the terrestrial biosphere: Ecosystem models and atmospheric observations. *Ecological Applications*, *10*(6), 1553–1573.

Prince, S. D., & Goward, S. N. (1995). Global primary production: A remote sensing approach. *Journal of Biogeography*, *22*(4/5), 815–835. https://doi.org/10.2307/2845983

Qiu, B., Chen, J. M., Ju, W., Zhang, Q., & Zhang, Y. (2019). Simulating emission and scattering of solar-induced chlorophyll fluorescence at far-red band in global vegetation with different canopy structures. *Remote Sensing of Environment*, *233*, 111,373. https://doi.org/10.1016/j.rse.2019.111373

Raupach, M. R. (1989). Applying Lagrangian fluid mechanics to infer scalar source distributions from concentration profiles in plant canopies. *Agricultural and Forest Meteorology*, *47*(2–4), 85–108.

Reichstein, M., Falge, E., Baldocchi, D., Papale, D., Aubinet, M., Berbigier, P., et al. (2005). On the separation of net ecosystem exchange into assimilation and ecosystem respiration: Review and improved algorithm. *Global Change Biology*, *11*(9), 1424–1439. https://doi.org/10.1111/j.1365-2486.2005.001002.x

Richardson, A. D., Hollinger, D. Y., Burba, G. G., Davis, K. J., Flanagan, L. B., Katul, G. G., et al. (2006). A multi-site analysis of random error in tower-based measurements of carbon and energy fluxes. *Agricultural and Forest Meteorology*, *136*(1–2), 1–18. https://doi.org/10.1016/j.agrformet.2006.01.007

Rocha, A. V., Potts, D. L., & Goulden, M. L. (2008). Standing litter as a driver of interannual CO_2 exchange variability in a freshwater marsh. *Journal of Geophysical Research*, *113*, G04020. https://doi.org/10.1029/2008JG000713

Ross, J. (1980). *The radiation regime and architecture of plant stands*. The Hague: Dr. W Junk.

Ruimy, A., Dedieu, G., & Saugier, B. (1996). TURC: A diagnostic model of continental gross primary productivity and net primary productivity. *Global Biogeochemical Cycles*, *10*(2), 269–285.

Running, S. W., Baldocchi, D. D., Turner, D., Gower, S. T., Bakwin, P., & Hibbard, K. (1999). A global terrestrial monitoring network, scaling tower fluxes with ecosystem modeling and EOS satellite data. *Remote Sensing of the Environment.*, *70*, 108–127.

Running, S. W., Nemani, R. R., Heinsch, F. A., Zhao, M. S., Reeves, M., & Hashimoto, H. (2004). A continuous satellite-derived measure of global terrestrial primary production. *Bioscience*, *54*, 547–560.

Ryu, Y., Baldocchi, D. D., Verfaillie, J., Ma, S., Falk, M., Ruiz-Mercado, I., et al. (2010). Testing the performance of a novel spectral reflectance sensor, built with light emitting diodes (LEDs), to monitor ecosystem metabolism, structure and function. *Agricultural and Forest Meteorology*, *150*(12), 1597–1606. https://doi.org/10.1016/j.agrformet.2010.08.009

Ryu, Y., Berry, J. A., & Baldocchi, D. D. (2019). What is global photosynthesis? History, uncertainties and opportunities. *Remote Sensing of Environment*, *223*, 95–114. https://doi.org/10.1016/j.rse.2019.01.016

Ryu, Y., Verfaillie, J., Macfarlane, C., Kobayashi, H., Sonnentag, O., Vargas, R., et al. (2012). Continuous observation of tree leaf area index at ecosystem scale using upward-pointing digital cameras. *Remote Sensing of Environment*, *126*, 116–125. https://doi.org/10.1016/j.rse.2012.08.027

Schaefer, K., Schwalm, C. R., Williams, C., Arain, M. A., Barr, A., Chen, J. M., et al. (2012). A model-data comparison of gross primary productivity: Results from the North American carbon program site synthesis. *Journal of Geophysical Research*, *117*, G03010. https://doi.org/10.1029/2012JG001960

Sellers, P. J. (1985). Canopy reflectance, photosynthesis and transpiration. *International Journal of Remote Sensing*, *6*(8), 1335–1372. https://doi.org/10.1080/01431168508948283

Sellers, P. J. (1987). Canopy reflectance, photosynthesis, and transpiration.2. The role of biophysics in the linearity of their interdependence. *Remote Sensing of Environment*, *21*(2), 143–183.

Sellers, P. J., Berry, J. A., Collatz, G. J., Field, C. B., & Hall, F. G. (1992). Canopy reflectance, photosynthesis, and transpiration.3. A reanalysis using improved leaf models and a new canopy integration scheme. *Remote Sensing of Environment*, *42*(3), 187–216.

Sims, D. A., Rahman, A. F., Cordova, V. D., Baldocchi, D. D., Flanagan, L. B., Goldstein, A. H., et al. (2005). Midday values of gross CO_2 flux and light use efficiency during satellite overpasses can be used to directly estimate eight-day mean flux. *Agricultural and Forest Meteorology*, *131*(1–2), 1–12. https://doi.org/10.1016/j.agrformet.2005.04.006

Sonnentag, O., Hufkens, K., Teshera-Sterne, C., Young, A. M., Friedl, M., Braswell, B. H., et al. (2012). Digital repeat photography for phenological research in forest ecosystems. *Agricultural and Forest Meteorology*, *152*, 159–177. https://doi.org/10.1016/j.agrformet.2011.09.009

Taddeo, S., & Dronova, I. (2018). Indicators of vegetation development in restored wetlands. *Ecological Indicators*, *94*, 454–467. https://doi.org/10.1016/j.ecolind.2018.07.010

Tucker, C. J. (1979). Red and photographic infrared linear combinations for monitoring vegetation. *Remote Sensing of Environment*, *8*(2), 127–150. https://doi.org/10.1016/0034-4257(79)90013-0

van der Tol, C., Verhoef, W., & Rosema, A. (2009). A model for chlorophyll fluorescence and photosynthesis at leaf scale. *Agricultural and Forest Meteorology*, *149*(1), 96–105. https://doi.org/10.1016/j.agrformet.2008.07.007

van der Tol, C., Verhoef, W., Timmermans, J., Verhoef, A., & Su, Z. (2009). An integrated model of soil-canopy spectral radiances, photosynthesis, fluorescence, temperature and energy balance. *Biogeosciences*, *6*(12), 3109–3129. https://doi.org/10.5194/bg-6-3109-2009

Verma, M., Schimel, D., Evans, B., Frankenberg, C., Beringer, J., Drewry, D. T., et al. (2017). Effect of environmental conditions on the relationship between solar-induced fluorescence and gross primary productivity at an OzFlux grassland site. *Journal of Geophysical Research: Biogeosciences*, *122*, 716–733. https://doi.org/10.1002/2016JG003580

Webb, E. K., Pearman, G. I., & Leuning, R. (1980). Correction of flux measurements for density effects due to heat and water-vapor transfer. *Quarterly Journal of the Royal Meteorological Society*, *106*(447), 85–100.

Xu, L., & Baldocchi, D. D. (2003). Seasonal trend of photosynthetic parameters and stomatal conductance of blue oak (*Quercus douglasii*) under prolonged summer drought and high temperature. *Tree Physiology*, *23*(13), 865–877. https://doi.org/10.1093/treephys/23.13.865

Yang, K., Ryu, Y., Dechant, B., Berry, J. A., Hwang, Y., Jiang, C., et al. (2018). Sun-induced chlorophyll fluorescence is more strongly related to absorbed light than to photosynthesis at half-hourly resolution in a rice paddy. *Remote Sensing of Environment*, *216*, 658–673. https://doi.org/10.1016/j.rse.2018.07.008

Yang, P., & van der Tol, C. (2018). Linking canopy scattering of far-red Sun-induced chlorophyll fluorescence with reflectance. *Remote Sensing of Environment*, *209*, 456–467. https://doi.org/10.1016/j.rse.2018.02.029

Yuan, W., Liu, S., Zhou, G., Zhou, G., Tieszen, L. L., Baldocchi, D., et al. (2007). Deriving a light use efficiency model from eddy covariance flux data for predicting daily gross primary production across biomes. *Agricultural and Forest Meteorology*, *143*(3–4), 189–207. https://doi.org/10.1016/j.agrformet.2006.12.001

Zeng, Y., Badgley, G., Dechant, B., Ryu, Y., Chen, M., & Berry, J. A. (2019). A practical approach for estimating the escape ratio of near-infrared solar-induced chlorophyll fluorescence. *Remote Sensing of Environment*. https://doi.org/10.1016/j.rse.2019.05.028

Zhao, M., Heinsch, F. A., Nemani, R. R., & Running, S. W. (2005). Improvements of the MODIS terrestrial gross and net primary production global data set. *Remote Sensing of Environment*, *95*(2), 164–176. https://doi.org/10.1016/j.rse.2004.12.011